Environ. Sci. Technol. **1998**, *32,* 2680−2687

Modeling Pyrite Oxidation in Arid Environments

G. G. FENNEMORE, W. CHAD NELLER, AND ANDY DAVIS*

Geomega, 2995 Baseline Road, Suite 202, Boulder, Colorado 80303

Understanding future pit lake water quality has become an important element in permitting open pit mines, due to the potential long-term water quality impacts on ecological receptors. Quantifying pyrite oxidation kinetics is an integral part of this analysis. To date, constraints resulting from low moisture content in the arid regions of the southwestern U.S. that host many large, disseminated deposits have not been considered. In this study, laboratory humidity cells routinely used to simulate pyrite reactivity were found to overestimate pyrite oxidation rates in arid environments by a factor of >2 compared to the same material emplaced in the field. Increasing particle size also resulted in decreasing reactivity, with 16−64 mm diameter grains <50% as reactive as 4−16 mm diameter grains. A pyrite oxidation model that incorporates both fracture and porous media pyrite oxidation using site-specific data, e.g., wall rock geometry, moisture content, etc., was developed to simulate wall rock reactivity in arid environments. The results demonstrated a 3-fold reduction in oxidized wall rock thickness in arid environments compared to assumptions of constant 100% moisture, with a concomitant reduction in solute loading to the incipient pit lake.

Introduction

Advances in milling and beneficiation techniques have resulted in the advent of open pit mining to recover metals from low-grade deposits. As a result, many of the economic reserves that extend in excess of 300 m beneath the ground surface require dewatering, with consequent depression of the groundwater table. After the deposit is exhausted, groundwater withdrawals cease, resulting in inundation of the excavation, and formation of a pit lake. In Nevada, it is anticipated that up to 30 of these water bodies may form over the next few decades (*1*). Predicting the potential water quality of the future pit lake is of particular importance due to regulatory concerns both in the U.S. (*2*), and abroad (*3*), related to water quality standards, potential impacts on avian receptors, and on local groundwater quality after the pit lake forms (*4*).

Many of the deposits consist of an oxide cap overlying sulfide-hosted mineralization juxtaposed against limestone units (Figure 1). Pyrite (FeS_2), pyhrrotite (FeS), and marcasite (FeS) in the pit wall has the potential to oxidize upon exposure to the atmosphere, generating acid and sulfate that contribute to solute loading of the pit lake as returning groundwater flushes salts from the pit wall rock (*4*). Conversely, alkalinity inherent in groundwater emanating from the generally more transmissive limestone units in the pit has the potential to react with acid in the water column, forming precipitates (*1, 4*), resulting in a metal-rich basal sludge (Figure 1).

To date, most research on pyrite oxidation kinetics has been conducted in the laboratory under saturated conditions (*5*−*7*). Although these studies are relevant in a temperate environment, they are of limited utility in the arid conditions characteristic of the desert southwestern U.S., where many large precious metal deposits occur, and a lack of moisture can reasonably be hypothesized to retard pyrite oxidation kinetics.

Exposure of mineralized rocks to the atmosphere in the ultimate pit surface (UPS) wall rock, represented by the rind of exposed wall rock at the perimeter and base of the excavation results in pyrite oxidation, primarily catalyzed by ferric iron (*8*), i.e.,

$$FeS_2 + 14Fe^{3+} + 8\ H_2O \Rightarrow 15Fe^{2+} + 2\ SO_4^{2-} + 16H^+ \quad (1)$$

Conversely, pyrite oxidation by oxygen is approximately an order of magnitude slower than by ferric iron (*9*). The sluggish reactivity of oxygen-mediated pyrite oxidation indicates that the rate of pyrite oxidation in an arid environment is contingent on the availability of moisture, rather than oxygen. However, to date pyrite oxidation models have been based on the diffusion of an oxidant through an oxide coating that grows as the pyrite core shrinks and have neglected the role of moisture.

In temperate environments, simplifying assumptions, i.e., that pyrite is evenly distributed in a uniform porous medium of particles represented by identically sized spheres, and that oxidation takes place in an aqueous environment where pyrite is continually bathed in a wetting solution with all pyrite surfaces exposed (*10, 11*), are appropriate. However, they are inappropriate for open pit wall rock conditions in an arid environment, where pyrite oxidation is primarily controlled by transport of air in fractures, as opposed to through porous media, and mitigated by incarceration within a refractory host (Figure 2).

Because the Davis−Ritchie model (*10*) does not account for moisture content, the oxidation depth of two identical pyritiferous rocks in an arid (<5% moisture content) and a humid (>25% moisture content) wall rock environment are indistinguishable in terms of oxidation zone thickness. In theory, the humid environment should result in a deeper oxidation front due to the presence of freely available moisture (eq 1). Recognition of this artifact led us to develop an approach that modifies the assumptions used to represent oxidation of pyrite in the arid pit wall rock environment. Specifically, oxygen diffusion in macrofractures, heterogeneous wall rock particle sizes, and moisture rate limitation were added to the Davis−Ritchie algorithm. Incorporating a water limitation term is particularly important because laboratory experiments have demonstrated that a lack of moisture will decrease the oxidation rate, and thus reduce solute mass transported from the rock (*12*).

This communication describes the model structure and its verification using field experimental data collected from two mining sites in Nevada. The oxidation model predicts the mass of sulfate and acid generated, and the thickness of the oxidation rind (the region of rock where the pyrite oxidation rate is negligible). These quantities are determined as a function of time, rock porosity, rock particle size, oxygen diffusion rate, water rate-limiting factor, and percent pyrite content.

Mathematical Formulation. Our approach incorporates the availability of oxygen and water required for acid

* Corresponding author tel: (303) 938-8115; fax: (303) 938-8123; e-mail: geomega@pcisys.net.

S0013-936X(97)00900-0 CCC: $15.00
Published on Web 08/12/1998

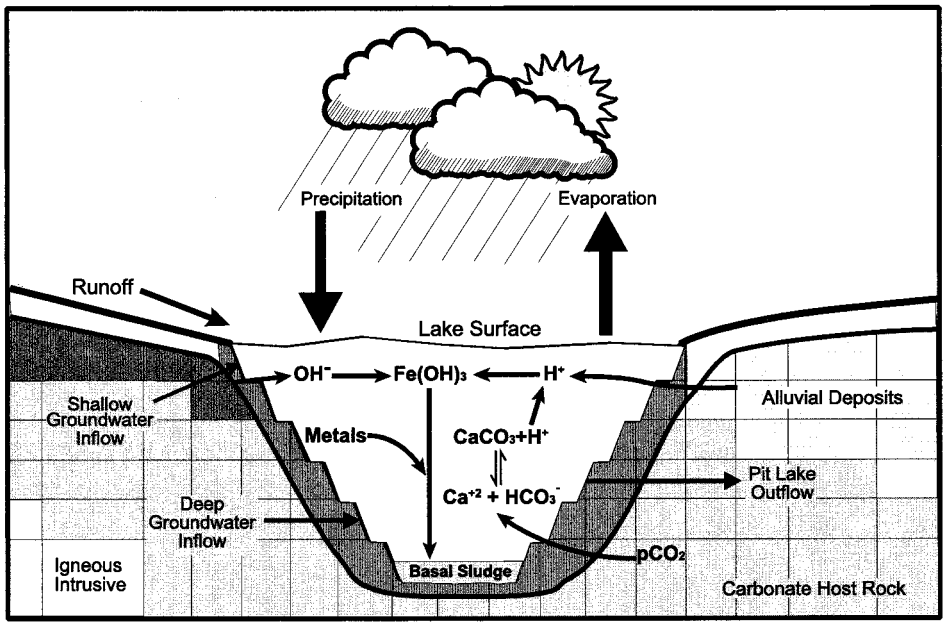

FIGURE 1. Physical and chemical mechanisms contributing to pit lake water chemistry can include pit refilling and hydrodynamics, wall rock oxidation, solute precipitation, and sorption to amorphous precipitates.

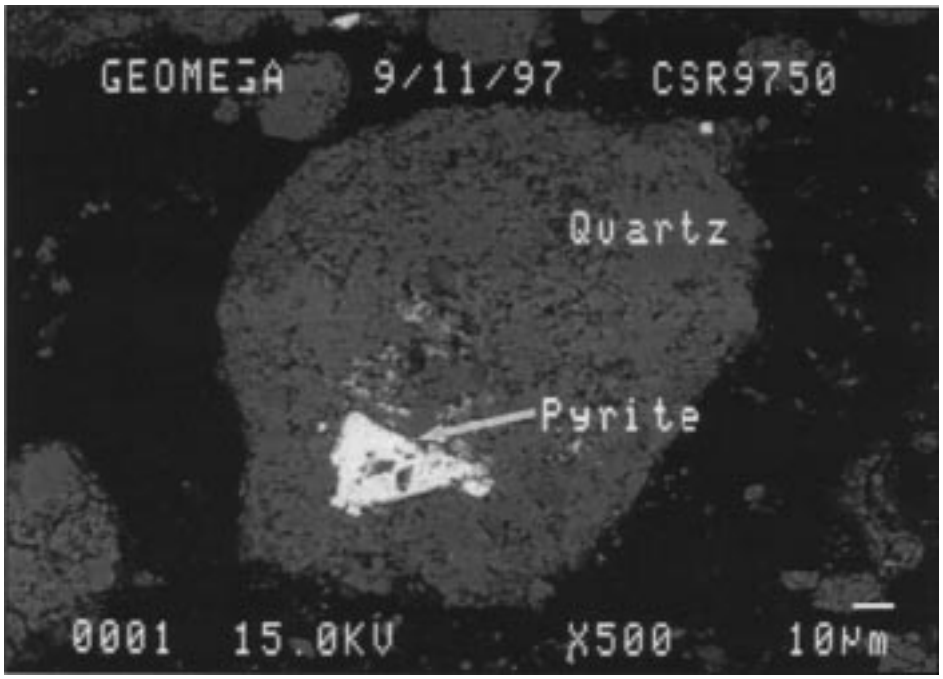

FIGURE 2. Pyrite encapsulated in refractory quartz from a sample of open pit wall rock.

generation, and the fracture-controlled geometry of the wallrock. Oxygen transport to pyrite is assumed to occur by diffusion from oxygen-filled wall rock fractures into pore space and then into the pyrite-hosting rock. The assumption of atmospheric oxygen in the wall rock fractures accounts for the transport of oxygen (advective and diffusive) into the wall rock via these preferential pathways. The rate of pyrite oxidation is modeled as a shrinking sphere where an oxidized shell expands to consume an unoxidized spherical core.

The model equations simulate pyrite oxidation based on transport of oxygen within the rock unit. The model consists of a system of four coupled equations incorporating oxygen diffusion; the oxidation rate; the oxidized volume; and sulfate release, modified from ref *10* to accommodate site-specific effects. A water rate-limiting term was added to the oxidation rate equation, and a "sink" term added to the oxygen diffusion equation (see Appendix for mathematical formulations).

The rate of oxygen diffusion and oxidation rate depend on the assumed water content of the rock matrix (*13*), i.e.,

$$D_1(\theta) = D_g^a \frac{(\phi - \theta)^{3.3}}{\phi^2} \quad (2)$$

where D_1 is the diffusion rate coefficient, D_g^a is the diffusion coefficient of oxygen in air, ϕ is the rock porosity, and θ is the rock water content. Therefore, oxygen diffusion is reduced as the system becomes saturated.

Numerical Approach. The model equations were solved to calculate oxidized thickness and sulfate release using a second-order, explicit, finite difference method with uniform

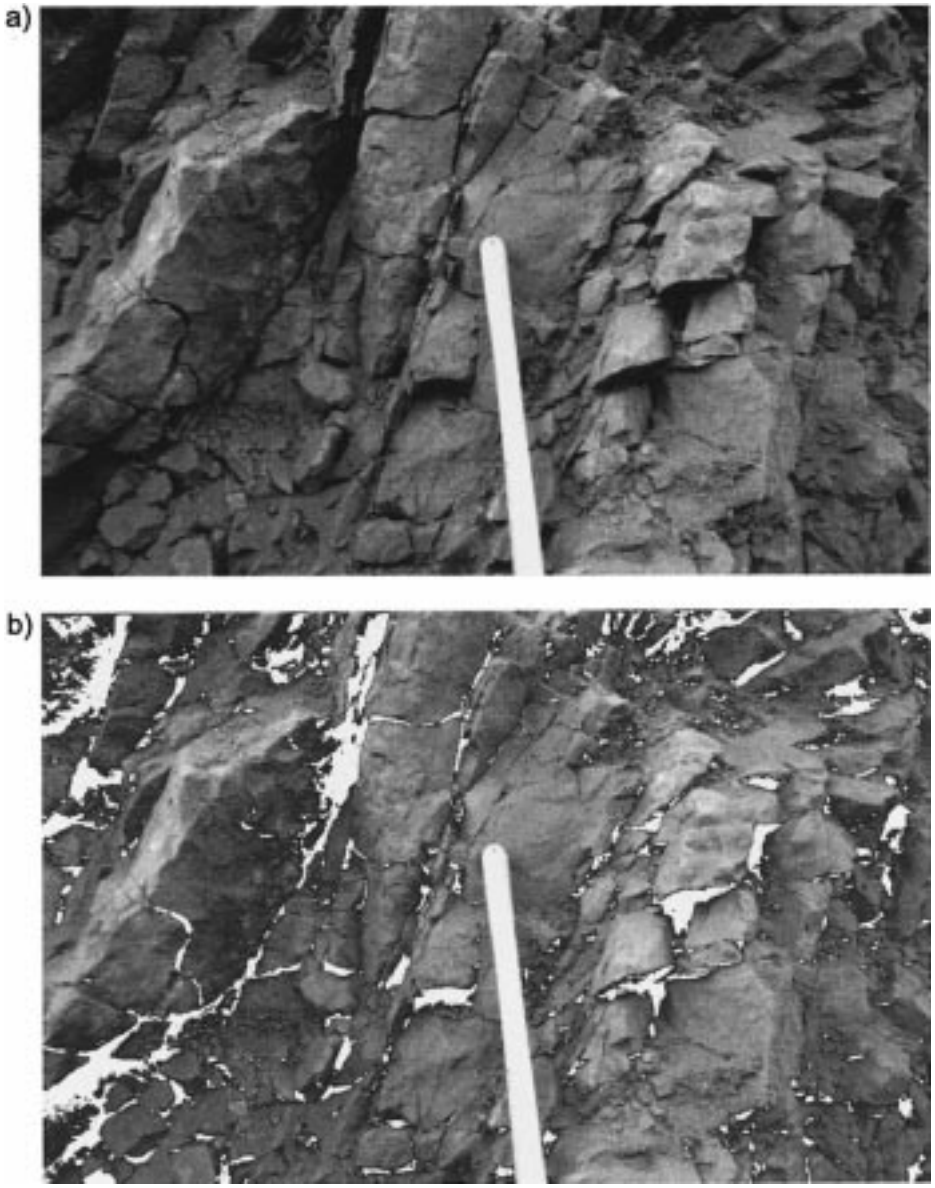

FIGURE 3. A photograph of open pit wall rock demonstrating the fracture density. The wall rock (a) was analyzed using image processing software to identify fractures (b). A shovel handle is included for scale.

spatial increments implemented as a FORTRAN code. Numerical methods were used rather than approximate analytical solutions to maximize solution rigor. An explicit solving routine was selected over implicit algorithms because explicit schemes have improved mass balance once stability criteria are met (*14, 15*).

Wall Rock Geometry. In addition to modifying the equations governing transport and reaction, the amended model also considers the geometry of the application. Initial efforts to model pyrite oxidation in wall rock assumed that the wall rock medium was uniform, with constant transport characteristics. However, visual inspection of wall rock in an open pit reveals considerable heterogeneity (Figure 3). During mining, blasting of benches shatters wall rock, leaving multiple macrofractures in the blast face that act as conduits, allowing penetration of atmospheric oxygen, and potentially oxidizing additional pyrite. Hence, the initial surface area exposed to oxidation in the amended model included both macrofractures and porous wall rock face surface.

An idealized distribution of macrofractures in the wall rock was assumed within 1.1 m of the blast surface (*16, 17*). Further into the wall rock, the effect of blasting diminishes and there are few macrofractures. Photogrammetric analysis of 54 wall rock photographs input into an image processing package (*18*) allowed determination of macrofracture density at the wall rock surface (*19*) using the ratio of fracture pixels to total pixels in the photograph (based on color differences) to compute the fracture pixel ratio. Because fracture density is represented as a fractal with a fractal dimension of 2.9 (*20*), an empirical relation relating the known macrofracture density of the wall rock face to the negligible density at the 1.1 m depth was derived that described the macrofracture density at intermediate depths, i.e.,

$$\rho_{\text{frac}}(x) = \rho_{\text{frac}}(0)\left(\frac{1.1 - x}{1.1}\right)^{-2.9} + \phi_{\text{rock}} \qquad (3)$$

where $\rho_{\text{frac}}(0)$ is the site-specific macrofracture density at the wall rock surface and ϕ_{rock} represents the porosity of the rock particles.

To model pyrite oxidation using the site-specific macrofracture distribution, it was assumed that atmospheric oxygen fills the macrofractures, hence the model domain was divided into several subdivisions, the relative size of

which was based on distance from the wall rock face, i.e.,

$$L(x) = \frac{\rho_{frac}(0)L_0}{\rho_{frac}(x)} \quad (4)$$

where $L(x)$ is the particle size as a function of depth, and L_0 is the particle size on the wall surface. Equation 4 was derived assuming fractures are distributed uniformly across the wall rock face because most fractures are due to relatively even stress applied to a rock face as a result of a uniform blasting pattern (*16*, *17*).

Thus, each wall rock section contains multiple small segments at the wall rock surface, intermediate-sized segments in the area behind the face, and a large segment beyond the 1.1 m depth. Assuming that macrofractures contain atmospheric oxygen, oxidation of each rock segment can be modeled independently. Accumulating the total oxidation region and sulfate release in each segment provides the total for the entire model domain. The accuracy of this technique was verified by determining a mass balance on oxygen and sulfur and duplicating previous results (*10*) using identical model domains and parameters (see Supporting Information).

Laboratory Tests. Humidity cell tests designed to oxidize pyrite under favorable conditions with sufficient available moisture and oxygen (*21*), together with field oxidation tests, were run on splits of rock samples collected from the Gold Quarry mine site, Elko, NV, and the Pipeline Project, Crescent Valley, NV. Rock acid generating potentials are described by the net carbonate value (NCV), i.e.,

$$\text{NCV} = 3.67 \times \%\ \text{carbonate} - 1.37 \times \%\ \text{sulfide} \quad (5)$$

where the coefficients represent the acid generating and neutralizing potentials in terms of $\%CO_2$. The rock samples covered a broad range of acid generating potentials with NCV values between −7 and +16 (Table 1). A matrix of 15 humidity cell tests with three particle size classifications (diameters between 2 and 4 mm, 4−16 mm, and 16−64 mm) for the five rock types was established (Table 1). Each humidity cell was loaded with 500 g of rock, and dry air passed through the cell for 3 days, followed by moist air for 3 days (*21*). On the seventh day, airflow was stopped, each cell leached with 500 mL of deionized water for 1 h, and the effluent collected and filtered through 0.45 μm membrane filters. Each cell was run for 20 cycles, with effluent from weeks 1, 2, 4, 8, 14, and 20 analyzed for the Nevada Profile I Analyte list (*22*) with laboratory measurements of pH, and spectrophotometric analysis of sulfate, total iron, and ferrous iron (*23*). A full data set is provided in the Supporting Information (see paragraph at end of paper).

Field Experiments. Rock samples were oxidized at the two mine sites using homogeneous splits of the 15 samples used in the humidity cells. Each sample (800 g) was placed in a field oxidation unit at the mine site and allowed to oxidize under ambient freeze−thaw and precipitation (rain/snow) conditions over a period of 8 months. Evaporation of leachate was precluded by use of a J-loop between the sample bucket and the collection bottle and the bottle shaded from exposure to sunlight to prevent temperature variations. Leachate from each bucket was collected after major precipitation events, the volume measured, and the fluid analyzed in the same manner as the humidity cells. Water samples were also collected from a control bucket containing no rock (see Supporting Information).

Results and Discussion

The humidity cell leachate chemistry collected from 10 L of water applied during 60 days under humid conditions over 20 weeks was compared with field leachate chemistry from an average of 11 L from six major precipitation events over 30 weeks. When normalized for fluid volume, these data demonstrate that, for any given particle size, the mass of solute leached was less in the field than in the humidity cell, and that, over equivalent time periods, the total mass leached was less from the larger particle sizes (Figure 4). In addition, the major ion chemistry of the humidity cell leachate became enriched in SO_4 and Cl (see Supporting Information) and also evolved over particle size (Figure 5).

The humidity cell leachates from rock type 1 were generally more acidic and contained higher sulfate concentrations than the field oxidation duplicates (Figure 4), demonstrating that pyrite oxidation in the humidity cells occurred more rapidly than in the site-specific field samples. Oxygen was freely available in both the humidity cells and buckets, hence we hypothesize that the difference in the oxidation rate was due primarily to ambient moisture content in Nevada that contrasts with generally saturated conditions in the humidity cells.

Model Calibration to Experimental Data. Parameter values for particle size (a), porosity (ϕ_{rock}), and percent pyrite content (ρ_{FeS}) were measured for each rock type prior to initiation of the study (Table 1), and an average surface fracture density, $\rho_{frac}(0) = 0.094$ determined from the photogrammetric analysis of pit wall rock. Parameter values for the oxygen diffusion rate in the atmosphere (D_g^a), atmospheric oxygen content (u_o), and stoichiometric constants from the pyrite reaction equation (ϵ), were obtained from the literature (Table 1). The remaining parameters required were the oxygen diffusion rate into the rock particles (D_2), and the water content rate-limiting factor ($\bar{\theta}$).

TABLE 1. Description of Rock Samples and Model Parameters

Rock Samples Used in Oxidation Experiments

rock type	particle size (mm)	porosity	%pyrite
1. carbonaceous siliceous refractory siltstone	2−4 4−16 16−64	0.008	1.17
2. oxidized siliceous siltstone	2−4 4−16 16−64	0.003	0.06
3. sulfitic siliceous refractory siltstone	2−4 4−16 16−64	0.007	5.07
4. unoxidized carbonaceous limestone	2−4 4−16 16−64	0.013	0.04
5. calcified, less-altered siltstone	2−4 4−16 16−64	0.038	0.01

Parameter Values Used in the Wall Rock Application

literature values	
atmospheric oxygen diffusion rate	2.25×10^{-5} m²/s (*23*)
atmospheric oxygen content	0.265 kg/m³
mass oxygen per mass sulfur oxidized	1.746
measured values	
percent pyrite, ρ_{SO_4}	rock-specific (see above)
rock porosity, ϕ_{rock}	rock-specific (see above)
surface fracture density, $\rho_{frac}(0)$	9.4%
assumed values	
humidity cell water content, θ	0.25
field oxidation water content, θ	0.05

Calibrated Values

rock type	oxygen diffusion, D_2 (m²/s)	water rate-limiting factor, $\bar{\theta}$
1	7×10^{-11}	0.25
2	2×10^{-13}	0.25
3	1×10^{-10}	0.50
4	1×10^{-12}	0.25
5	5×10^{-13}	0.50

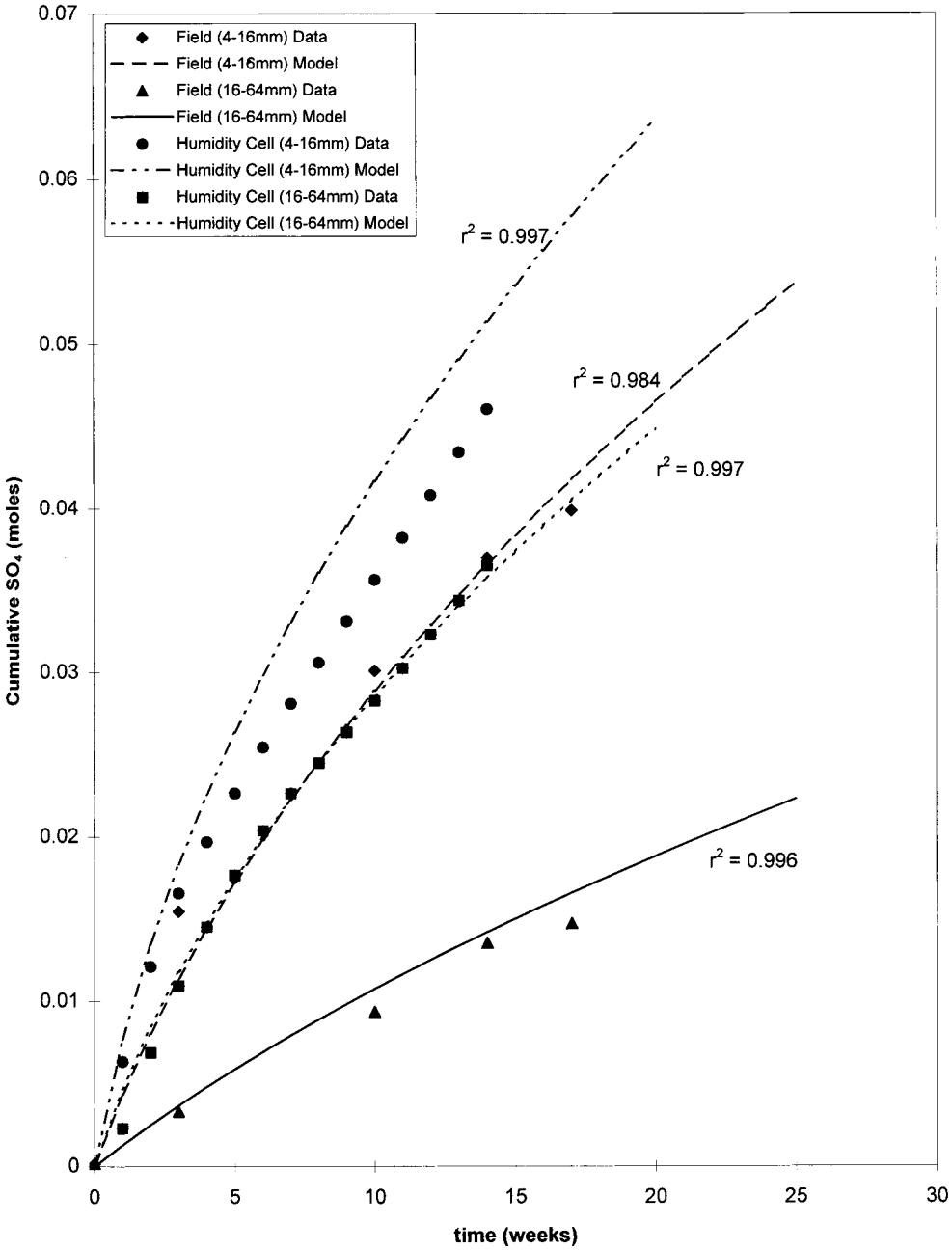

FIGURE 4. Sulfate leached from the acid-generating sulfitic siliceous refractory rock for the field and humidity cell with the associated model results. r^2 statistics are shown to quantify the fit to the analytical data.

Humidity Cell Data. No water rate-limiting effects were included in modeling the humidity cell tests ($\bar{\theta} = 1$); therefore, the sulfate concentrations in cell leachate were used to calibrate an oxygen diffusion rate that excluded constraints on water availability. A value for D_2 was determined from the largest particle size for each rock type by adjusting D_2 until predicted sulfate releases matched the experimental data. To verify this value, the diffusion rate was held constant while the particle size parameters were decreased to match the two smaller particle sizes for each rock type. In general, identical oxygen diffusion rates resulted in good agreement with the analytical data ($r^2 > 0.95$) for the different particle sizes (Figure 4), demonstrating that the value selected for the oxygen diffusion rate was representative of the true diffusion rate through each rock type.

Field Oxidation Experiments. After using the humidity cell tests to calibrate the oxygen diffusion rate, the sulfate concentrations from the field oxidation tests were corrected for the control bucket contributions to determine the water content rate-limiting factor. The oxygen diffusion rate and particle size were held constant at the level determined from the humidity cell simulations for each rock type and particle size in the field oxidation tests, and the model was calibrated to the field oxidation data by adjusting $\bar{\theta}$ in the model equations (Appendix). This fit resulted in improved simulations of the lower reaction rates observed in the field experiment compared to the humidity cell data (Figure 4).

Wall Rock Application. Following verification, the model was used to determine the oxidized thickness of arid wall rock comprised of carbonaceous siliceous refractory siltstone under moisture conditions observed at the site-specific field test. The pyrite content and rock porosity were 1.17% and 0.008, respectively (Table 1). Particle size and fracture density of the rock face were measured photogrammetrically with values for these parameters with depth behind the wall rock face determined using fractal functions (eqs 3 and 4). D_2

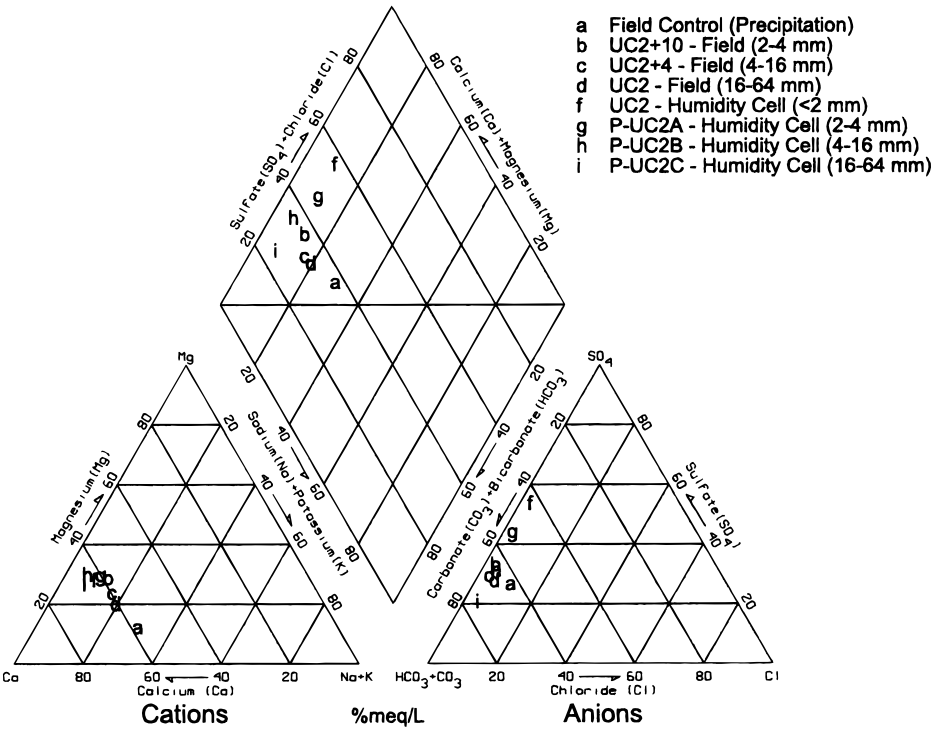

FIGURE 5. Analytical data collected from the field and laboratory tests plotted on a Piper diagram. The leachate chemistry from the field oxidation test from the largest (16−64 mm) particle size (point d) is closest to the incident-precipitation chemistry (point a) whereas the leachates from the 4−16 mm (point c) and 2−4 mm (point b) particles sizes are successively closer to the chemistry observed in humidity cell tests (points f, g, h, and i).

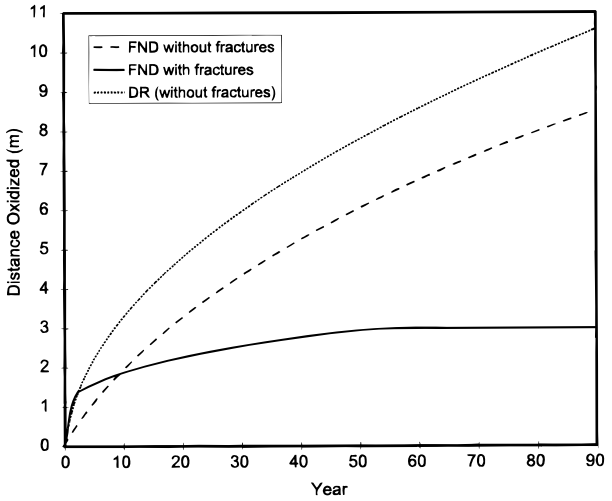

FIGURE 6. Predicted oxidation thicknesses in open pit wall rock using the Davis-Ritchie numerical code, the proposed model with fracture control of oxygen diffusion, and the proposed model in the absence of fracture control.

and $\bar{\theta}$ were determined by calibration to the humidity cell and field oxidation experiments as described above.

This study identifies the need for an explicit derivation of $\bar{\theta}$ as a function of humidity using pyrite oxidation tests at several water contents. Using these inputs, the model proposed here predicts more rapid initial oxidation than the Davis−Ritchie model (*10*), due to the incorporation of macrofractures that initially expose more rock surface area to oxygen (Figure 6). After three years, oxidation rates decrease due to site-specific water limitations and the reduction in fracture density, as macrofractures diminish with depth into the rock wall. A sensitivity analysis (see Supporting Information) of the wall rock application indicated that the model is most sensitive to variation in the D_2 parameter.

This model facilitates incorporation of site-specific data, e.g., wall rock geometry and water content rate control, together with calibration to laboratory and field oxidation experiments. The results demonstrate a 3-fold reduction in oxidized wall rock thickness (Figure 6) in arid environments (compared to assumptions of constant 100% moisture) with a concomitant reduction in solute loading to the incipient pit lake.

Acknowledgments

The authors would like to thank Dr. G. B. Davis for providing the original numerical code used in evaluating the Davis−Ritchie approach. We appreciate the assistance of S. Helgen for assistance in model conceptualization and Dr. L. E. Eary, M. Leslie, C. Tabor, A. Tisdale, and Dr. D. Stone for their assistance in gathering the experimental data. Funding for this research was provided by Newmont Gold Company, Placer Dome U.S. and BHP. The comments of Dr. J. Pankow and two anonymous reviewers resulted in substantial improvements in the manuscript. A.D. appreciates the support of Kathy Davis over this period.

Appendix

Oxidation modeling based on the results of the site-specific experiments (e.g., humidity cell and field tests) was conducted using fixed moisture contents representative of the degree of saturation observed in those tests (Table 1). The uniform moisture facilitated oxidation model calibration through formulation and solution of the model equations in dimensionless form. Written in dimensionless form, the model equations represent oxygen diffusion through the rock matrix, i.e.

$$\delta_1 u_t(x,t) = u_{xx}(x,t) - \frac{3k_1 u(x,t)\bar{\theta}R(x,t)}{1 - R(x,t)} \qquad \text{(A1)}$$

the rate of oxidation

$$R_t(x,t) = \frac{-k_1 u(x,t)\bar{\theta}}{R(x,t)[1 - R(x,t)]} \quad \text{(A2)}$$

an equation for the oxidized volume of wall rock

$$\text{vol}(t) = \int_0^L \frac{4}{3}\pi[R(x,0) - R(x,t)]^3 \, dx \quad \text{(A3)}$$

and an acid generation equation

$$SO_4(t) = \frac{\rho_{FeS_2}\text{vol}(t)}{2M_{FeS_2}} \quad \text{(A4)}$$

where

$u(x,t)$ = the oxygen concentration as a function of time and depth,

$R(x,t)$ = the radius of the unoxidized pyrite grains,

δ_1 = the dimensionless diffusion coefficient for air in wall rock,

θ = the relative water content of the rock,

$\bar{\theta}$ = the rate-limiting effect due to water content,

$D_1(\theta)$ = the diffusion coefficient for air into rock,

u_o = atmospheric oxygen content,

$\varepsilon = 1.746$, the mass of oxygen used per mass of sulfur oxidized,

ϕ = the wall rock porosity,

$k_1 = \dfrac{3\gamma D_2(1 - \phi)L^2}{D_1(\theta)a^2}$ is the oxidation rate constant,

$\gamma = 0.03$ is the gas law proportionality constant,

D_2 is the diffusion coefficient for air through rock particles,

L is the depth of the wall rock,

a is the particle size of the wall rock,

$SO_4(t)$ = cumulative moles of sulfate produced,

ρ_{FeS_2} = density of pyrite,

vol(t) = volume of oxidized rock, and

M_{FeS_2} = molecular weight of pyrite.

These equations were solved with the following initial and boundary conditions:

$$u(x,0) = 0$$

$$u(0,t) = 1$$

$$u_x(L,t) = 0$$

$$R(x,0) = 1$$

Numerical solutions were obtained from

$$\frac{u_i^{j+1} - u_i^j}{\Delta t} = \frac{1}{\delta_1}\left[\frac{u_{i+1}^j - 2u_i^j + u_{i-1}^j}{(\Delta x)^2} - \frac{3k_1 u_i^j \bar{\theta} R_i^j}{1 - R_i^j}\right] \quad \text{(A5)}$$

$$\frac{R_i^{j+1} - R_i^j}{\Delta t} = -\frac{k_1 u_i^j \bar{\theta}}{R_i^j(1 - R_i^j)} \quad \text{(A6)}$$

Solutions generated by this numerical scheme were benchmarked by comparison to the original Davis and Ritchie numerical code.

A feasible extension of the model to account for variable water content within the wall rock involves coupling eqs A1 and A2 with the variably saturated flow equation (Richard's equation)

$$\theta_t = [D[\theta(x,t)]\theta_x(x,t) - K[\theta(x,t)]]_x \quad \text{(A7)}$$

using the initial, boundary value conditions: $\theta(x,0) = \theta_r$ = the residual wall rock water content, $\theta(L,t) = \theta_s$ = the saturated water content of the bedrock at the water table, located at distance L, and $\theta_i(0,t) = f(t)$ = a time varying flux representing precipitation and evaporation from the wall rock surface that may be obtained from site-specific meteorological data (e.g., ref *24*).

The variably saturated flow equation is weakly coupled to the oxygen transport and reaction equations and does not depend on their solutions. However, if moisture content within the oxidizing wall rock varies significantly from either the humid or arid states, supplemental tests at intermediate moisture contents are necessary to define an empirical function relating the water rate-limitation factor and water content, $\bar{\theta}[\theta(x^*,t^*)]$.

Assuming that diffusion into rock particles is steady state (*10*), the dimensional form of eq A1 becomes

$$\varphi u_{i^*}^* = [D_1[\theta[x^*,t^*)]u_{x^*}^*]_{x^*} - 4\pi a^2 \gamma D_2 \theta[\theta(x^*,t^*)]\frac{u^* R^*}{(1 - R^*)a^2} \quad \text{(A8)}$$

Several explicit and implicit numerical schemes to this type of nonlinear, parabolic diffusion-reaction equation have been posited (*14*, *15*, *26*) including

$$\phi\frac{u_i^{j+1} - u_i^j}{\Delta t} = \frac{1}{\Delta x}\left[\frac{D_1(\theta_{i+1}^j) + D_1(\theta_i^j)}{2}\left(\frac{u_{i+1}^j - u_i^j}{\Delta x}\right) - \frac{D_1(\theta_i^j) + D_1(\theta_{i-1}^j)}{2}\left(\frac{u_i^j + u_{i-1}^j}{\Delta x}\right)\right] - 4\pi\gamma D_2 \bar{\theta}(\theta_i^j)\frac{u_i^j R_i^j}{(1 - R_i^j)} \quad \text{(A9)}$$

that yields mass-balanced results but is not the most computationally efficient (*15*, *25*).

Supporting Information Available

Tables of field oxidation and humidity cell data and figures of model sensitivity (43 pages). See any current masthead page for ordering information.

Literature Cited

(1) Miller, G. C.; Lyons, W. B.; Davis, A. *Environ. Sci. Technol.* **1996**, *30*, 118−123.

(2) U.S. Department of the Interior, Bureau of Land Management. *Cortez Pipeline* Gold Deposit: Final Environmental Impact Statement, 1996.

(3) Newmont Gold Company. *Impact Analysis for the Batu Hijau Copper/Gold Mining Project*, 1995.

(4) Davis, A.; Eary, L. E. *Mine Eng.* **1997**, *6*, 98−102.

(5) Nicholson, R. V.; Gillham, R. W.; Reardon, E. J. *Geochim. Cosmochim. Acta* **1990**, *54*, 395−402.

(6) Williamson, M. A.; Rimstidt, J. D. *Geochim. Cosmochim. Acta* **1994**, *58*, 5443−5454.

(7) Moses, C. O.; Herman, J. S. *Geochim. Cosmochim. Acta* **1991**, *55*, 471−482.

(8) Luther, G. W. *Geochim. Cosmochim. Acta* **1987**, *51*, 3193−3199.

(9) Nordstrom, D. *Acid Sulfate Weathering*; Soil Science Society of America: Madison, WI, 1982.

(10) Davis, G. B.; Ritchie, A. I. M. *Appl. Math. Modeling* **1986**, *10*, 314−322.

(11) Blowes, D. W.; Jambor, J. L. *Appl. Geochem.* **1990**, *5*, 327−346.

(12) Borek, S. L. *Environmental Geochemistry of Sulfide Oxidation*; *Effect of Humidity on Pyrite Oxidation*. pp 31−44, American Chemical Society Symposium Series, American Chemical Society: Washington, DC, 1994; Chapter 3, pp 31−44.

(13) Milligan, R.; Quirk, J.; *Nature* **1964**, *202*, 143−145.

(14) Dahlquist, G.; Bjork, A. *Numerical Methods*; Prentice-Hall: Englewood Cliffs, NJ, 1974.

(15) Fletcher, C. A. J. *Computational Techniques for Fluid Dynamics*; Springer-Verlag: New York, 1991; Vol. 1.

(16) Siskind, D. E.; Fumart, R. R. *Blast-produced fractures in Lithonia granite*; U. S.Department of the Interior, 1974.
(17) Chakrabory, A. K.; Jethwa, J. L.; Paithankar, A. G. *Tunneling Underground Space Technol.* **1994**, *9*, 471−482.
(18) Blin-LaCroix, J.; Thomas, A. *Eng. Geol.* **1990**, *28*, 171−190.
(19) Adobe PhotoShop version 4.0, 1996.
(20) Kozak, E.; Pachepshy Y. A.; Sokolowski, S.; Sokolowska, Z.; Stepniewski, W. *Soil Sci. Soc. Am. J.* **1996**, *60*, 1291−1297.
(21) Sobeck, A. A.; Schuller, W. A., Freeman, J. R.; Smith, R. M. *Field and laboratory methods applicable to overburdens and minesoils*; PD-280 495, U.S. Department of Commerce, National Technical Information Service, 1978.
(22) Nevada State Health Laboratory, Nevada Division of Environmental Protection Profile I Analyte List, 1996.
(23) Hach Company. *Hach DR/2000 Spectrophotometer Procedures Manual*; 1994.
(24) EarthInfo. *NCDC Hourly and 15 min Precipitation*; EarthInfo, Inc.: Boulder, CO, 1996.
(25) Sod, G. A. *Numerical Methods in Fluid Dynamics*; Cambridge University Press: Cambridge, U.K., 1985.

Received for review October 13, 1997. Revised manuscript received June 15, 1998. Accepted June 29, 1998.

ES970900O